HHS Public Access

Author manuscript

Transl Res. Author manuscript; available in PMC 2019 February 01.

Published in final edited form as:

Transl Res. 2018 February ; 192: 30–45. doi:10.1016/j.trsl.2017.10.007.

Peripheral Vascular Atherosclerosis in a Novel PCSK9 Gain-of-Function Mutant Ossabaw Miniature Pig Model

Ahmad F. Hedayat[1], **Kyoung-Ha Park**[2], **Taek-Geun Kwon**[3], **John R. Woollard**[1], **Kai Jiang**[1], **Daniel F. Carlson**[4], **Amir Lerman**[5], and **Lilach O. Lerman**[1,5]

[1]Division of Nephrology and Hypertension, Mayo Clinic, Rochester, MN, USA

[2]Division of Cardiovascular Diseases, Hallym University Medical Center, Anyang, South Korea

[3]Heart Center, Konyang University Hospital, Daejeon, South Korea

[4]Recombinetics Inc., St. Paul, MN, USA

[5]Division of Cardiovascular Diseases, Mayo Clinic, Rochester, MN, USA

Abstract

Hypercholesterolemia is a major risk factor for atherosclerosis. Remaining challenges in the management of atherosclerosis necessitate development of animal models that mimic human pathophysiology. We characterized a novel mutant pig model with DNA transposition of D374Y gain-of-function (GOF) cDNA of chimp proprotein convertase subtilisin/kexin type-9 (*PCSK9*), and tested the hypothesis that it would develop peripheral vascular remodeling and target organ injury in the kidney. Wild-type (WT) or PCSK9-GOF Ossabaw miniature pigs fed a standard or atherogenic diet (AD) (n=7 each), were studied in-vivo after 3- and 6-months of diet. Single-kidney hemodynamics and function were studied using multidetector computed-tomography, and kidney oxygenation by blood oxygen level-dependent magnetic-resonance-imaging. The renal artery was evaluated by intravascular ultrasound, aortic stiffness by MDCT, and kidney stiffness by magnetic resonance elastography. Subsequent ex-vivo studies included the renal artery endothelial function and morphology of abdominal aorta, renal, and femoral arteries by histology. Compared with WT, PCSK9-GOF pigs had elevated cholesterol, triglyceride, and blood pressure levels at 3- and 6-months. Kidney stiffness increased in GOF groups, but aortic stiffness only in GOF-AD. Hypoxia, intra-renal fat deposition, oxidative stress and fibrosis were observed in both GOF groups, whereas kidney function remained unchanged. Peripheral arteries in GOF groups showed medial thickening and development of atheromatous plaques. Renal endothelial function was impaired only in GOF-AD.

*Corresponding author: Lilach O. Lerman, MD, Ph.D., Division of Nephrology and Hypertension, Mayo Clinic, 200 First Street SW, Rochester, MN 55905, USA. Tel: +1 (507)-266-9376; Fax: +1 (507)-266-9316. lerman.lilach@mayo.edu.

Conflicts of Interest: All authors have read the journal's policy on disclosure of potential conflicts of interest.

Therefore, the PCSK9-GOF mutation induces rapid development of atherosclerosis in peripheral vessels of Ossabaw pigs, which is exacerbated by a high-cholesterol diet. This model may be useful for preclinical studies of atherosclerosis.

Keywords

PCSK9; Atherosclerosis; Cholesterol; Ossabaw; Kidney

INTRODUCTION

Atherosclerosis is responsible for coronary and peripheral artery disease, which can remain asymptomatic for decades.[1] Despite advances in medical, interventional, and surgical treatment, atherosclerotic disease is still the leading cause of death in both developed and developing countries.[2] Animal studies have revealed fundamental mechanisms by which low-density lipoprotein cholesterol (LDL-C) causes atherosclerosis, but numerous challenges remain regarding optimal management and understanding of the disease.[3]

Using animal models for understanding the pathophysiology of atherosclerosis and developing treatment or diagnostic strategies has proven somewhat challenging. Genetically modified mouse models have increased the understanding of the mechanisms and role of signaling pathways and genetic factors, which are important contributors to coronary artery disease and development of vascular disease. However, many models do not adequately replicate human disease, and their small size restricts clinically-applicable intravascular interventions and noninvasive imaging.[4, 5] Additionally, many key features of human atherosclerosis are rarely seen, particularly development of peripheral vascular disease. These limitations necessitate development of novel models to assess atherosclerotic features and management, as well as validating new treatments and devices.

Pigs can develop spontaneous atherosclerosis, which similar to humans is accelerated by an atherogenic diet,[6, 7] yet in normal pigs the lesions are generally minimal.[8] However, recent progress in genetic engineering has paved the way for the creation of new models by genetic manipulations. Proprotein convertase subtilisin/kexin type-9 (PCSK9) plays a key role in the clearance of LDL-C via its interaction with, and subsequent degradation of, LDL receptor (LDLR).[9] Following its discovery in 2003, a quest was started for both new gain-of-function (GOF) and loss-of-function mutations including D374Y PCSK9 and the heterozygote African nonsense C679X variants, respectively.[10, 11] GOF mutations result in greater binding of PCSK9 with LDL-R and increased LDL-C blood level. In addition to the PCSK9 enzyme, cholesteryl ester transfer protein (CETP), HMG-CoA reductase (HMGCR), peroxisome proliferator-activated receptor (PPAR)-α protein, and microsomal triglyceride transfer protein (MTTP) play an important role in the metabolism of lipids. In particular, the PCSK9 and CETP genes are both regulated by the SREBP transcription factor family.[12,13] CETP facilitates the transport of cholesteryl ester from high-density lipoprotein (HDL) to apolipoprotein B-containing lipoproteins, such as very low-density lipoprotein (VLDL) and LDL. CETP decreases the concentration of LDL-C and increases the concentration of HDL-C. PCSK9 may also affect plasma triglyceride via metabolism of

VLDL-C and their remnants,[14] but this overall effect is considered modest. Yet given the rapid developments in PCSK9 inhibition, analogous PCSK9-related approaches might be discovered for inhibition of triglyceride as well.[15]

Most of the genetically modified pig models have been developed by gene editing in porcine somatic cells followed by animal cloning.[16, 17] Al-Mashhadi et al. described development of hypercholesterolemia and atherosclerosis in PCSK9-GOF Yucatan minipigs.[18] Recently, we generated a novel D374Y human PCSK9-GOF Ossabaw pig model created by transposition of chimp DNA. Ossabaw pigs have the highest levels of total body lipid of any mammal even in the absence of a high-fat diet, and are naturally prone for spontaneous development of vascular disease. Furthermore, Ossabaw pigs fed a high-fat cholesterol diet develop hypertriglyceridemia and increased LDL:HDL cholesterol ratio, mild hypertension, and coronary artery disease.[19] Therefore, a combination of the Ossabaw pig genetic background with PCSK9-GOF could constitute a particularly promising model for vascular translational research.

The kidney is a common target organ in cardiovascular disease. Atherosclerotic changes in the renal artery are evident in 50% of patients with atherosclerotic disease elsewhere.[20] In addition to vascular remodeling, a growing body of evidence suggests that atherosclerosis has direct effects on the kidney, eliciting intrarenal microvascular and glomerular disease, positioning the kidney as an important target organ in peripheral vascular disease.[21] In the present study we characterized the PCSK9 Ossabaw pig model and tested the hypothesis that pigs with PCSK9-GOF mutation fed with a high-fat diet would develop peripheral vascular remodeling and renal injury.

MATERIALS AND METHODS

Study Protocols

This study was approved by the Mayo Clinic Institutional Animal Care and Use Committee. Twenty-one 3-mo-old female Ossabaw pigs (Recombinetics Inc., St. Paul, MN) were studied in 3 groups (n=7 each) including wild-type (WT) fed a normal diet (ND), PCSK9-GOF fed ND, and PCSK9-GOF fed an atherogenic diet (AD), all for 6-months. The AD diet was fed ad libitum (Agri-Nutrition Services, Inc., Shakopee, MN) and contains approximately 19.8% fat (ether extract, with 2% cholesterol), 17% protein, 5.3% fiber, and 41.8% carbohydrate (nitrogen-free extract by subtraction), with an estimated total average daily consumption of 6200 kcal (1020 kcal protein, 2674 kcal fat, and 2506 kcal carbohydrates).

At baseline, the animals were also implanted with a PhysioTel® telemetry transmitter (DSI, St. Paul, MN) for measurements of blood pressure. In-vivo imaging studies were performed after 3-months and repeated after 6-months of diet. For in-vivo studies, pigs were anesthetized and 8F sheaths placed in the jugular vein and artery to collect blood for lipid levels. Kidney function was quantified using multi-detector computed-tomography (MDCT) and the renal artery plaque volume (PV) by intravascular ultrasound (IVUS). Renal oxygenation was assessed in vivo by blood oxygen level-dependent magnetic resonance imaging (BOLD-MRI), renal stiffness by magnetic resonance elastography (MRE), and aortic distensibility evaluated by MDCT.

After the last 6-month in-vivo study the animals were allowed a 3-day recovery period, and were subsequently euthanized by a lethal intravenous dose of pentobarbital (Fatal-Plus solution, 100 mg/kg, Vortech, Dearborn, MI). The kidneys were removed, and sections frozen in liquid nitrogen (and maintained at −80°C) or preserved in formalin for in-vitro studies. In addition, kidney samples were prepared for microvascular architecture assessment with micro-CT. Histology sections were stained with Picro-sirius red, ox-LDL, Oil-Red-O, Terminal deoxynucleotidyl transferase dUTP nick-end labeling (TUNEL) and dihydroethidium (DHE), and examined by light microscopy to quantify fibrosis, fat deposition, apoptosis, and oxidative stress in the kidney.[22] Renal arteries were dissected to assess endothelial function, and the lower abdominal aorta, renal and femoral arteries isolated and stained with H&E, trichrome, Sirius-Red, Movat, CD107a and E06 to examine their morphology inflammatory infiltrates, and media-to-lumen ratio (M/L) ex vivo.

To distinguish the effect of GOF on PCSK9 and lipid levels from that of the AD alone, systemic in vivo data were collected from 3 additional WT pigs after a 6-months AD.

Systemic measurements

Mean arterial pressure (MAP) was measured as the average of the last 48 hours recorded by telemetry before each in-vivo study. Heart rate was monitored and recorded during MRI and MDCT studies. Levels of total cholesterol, triglycerides, LDL-C, and HDL-C were determined by standard procedures. VLDL-C was approximated as triglyceride/5 based on the Friedewald's, for our samples with triglyceride levels <400mg/mL.[23] PCKS9 plasma levels were measured by enzyme-linked immunosorbent assay (R&D, Minneapolis, MN). Urine was collected via bladder puncture to determine albumin excretion, and blood from the inferior vena cava for creatinine levels following standard procedures.

PCSK9 GOF Model Characterization

The primate coding sequence for PCSK9 that is 99% identical to H. sapiens, was introduced into male Ossabaw fibroblasts,[24] containing the mutation causing D374Y substitution. Transgenic cells were used for cloning to generate a transgenic Ossabaw founder line. Expression of PCSK9-D374Y transcript in these animals is directed by a liver-specific promoter to control PCSK9 expression to the liver, the primary endogenous source.[25]

In-Vivo Studies

Each in-vivo study consisted of MRI followed by MDCT studies 2–3 days later. For each study animals were weighed and then induced with 0.5 mg intramuscular ketamine and xylazine, intubated, and ventilated with room air. During MDCT, anesthesia was maintained with intravenous ketamine (0.2 mg/kg per minute) and xylazine (0.03 mg/kg per minute) and during MRI using isoflurane (1–2%) inhalation.

BOLD-MRI—To assess intra-renal oxygenation, BOLD-MRI was performed at 3T (Signa EXCITE, GE Healthcare, Waukesha, WI) using a spoiled gradient echo sequence as described previously[26, 27] R_2*, an index of deoxyhemoglobin concentration in cortical and medullary regions of the kidney, was quantified using an in-house developed MatLab software (MatLab 7.10, The MathWorks, Natick, MA). All scans were performed during

breath hold and regions of interest (ROI) manually traced in the cortex and medulla on the 7-ms echo time images to compute the average of MR signals within each ROI, and calculate R_2*.

MDCT—MDCT (Somatom Definition-128, Siemens Medical Solution, Forchheim, Germany) scanning was performed to assess kidney volume, renal blood flow (RBF) and glomerular filtration rate (GFR), as described previously,[28, 29] following a central venous injection of iopamidol (0.5 ml/kg/2 seconds). MDCT images were reconstructed and displayed on the Analyze™ software package (Biomedical Imaging Resource, Mayo Clinic, Rochester, MN). For functional data analysis, ROIs were selected from cross-sectional kidney images to generate time-attenuation curves and obtain measures of renal function. RBF was measured as the sum of the products of cortical and medullary perfusions and volumes, while GFR was calculated from the cortical curve using the slope of the proximal tubular curve. A separate cardiac scan was used to measure cardiac output[28] for calculation of systemic vascular resistance (SVR) as 80×MAP/Cardiac output.

Computed Tomography Angiography (CTA)—Computed tomography angiography (CTA) images of the renal artery were obtained using MDCT. Renal volume study was performed after a 15-min rest in the helical mode (240 mAs, 120 kV, pitch of 1.2, and B40 medium kernel) to obtain contiguous 5-mm-thick slices for measurements of cortical, medullary, and total kidney volume.

For CTA, the volume data was reconstructed at a resolution of 0.39×0.39 mm and 0.6 mm slice thickness with 0.3 mm overlap.[30] Automated quantification of diameter stenosis was acquired. A fast vessel-tracking algorithm was performed to acquire a 3-dimensional centerline of the renal artery and a stretched multiplanar-reformatted (MPR) volume created from the segment of interest, to allow studying the curved renal arteries as straight vessels. MPR volume-derived longitudinal and transverse outlines, detected by an initial approximation of the lumen border locations, were established by an automatic algorithm, with only limited manual input used to refine the automated processing steps. Then the lumen border outlines were detected in each transversal slice of the MPR volume with a circular lumen model. During this step, the intersection points of each transversal slice with the earlier obtained longitudinal outlines were used to guide the outline detection in each particular slice. Based on the cross-sectional area of the obtained transversal outlines, a diameter function along the vessel course was derived using the formula for circular cross sections.[31] Lastly, from these data, the reference diameter function, minimal lumen diameter, and degree of stenosis were obtained.

MRE—MRE scanning was performed during 30-second breath holds to assess medullary fibrosis in-vivo, as described previously.[32] We have shown that medullary stiffness provides a more reliable index of kidney fibrosis than cortical stiffness.[32] Briefly, Pigs were placed on their backs, and a 3D stack of images was collected using echo-planar imaging (EPI) in conjunction with motion-sensitizing gradients placed on the animal's dorsal surface, proximal to the kidneys. Images were analyzed using MRE/Wave (MRI Research Lab, Mayo Clinic, Rochester, MN). Measurements of tissue displacement were used to derive shear modulus. Stiffness values were averaged within ROIs, manually traced

around the renal medulla on the EPI magnitude images, and verified with the aid of co-registered contrast-enhanced MDCT images.

IVUS—After intravascular administration of 0.1mg/ml nitroglycerin, IVUS was performed using a 20 MHz IVUS catheter (Eagle Eye Gold, Volcano, Rancho Cordova, CA) that was inserted into the renal artery with an automatic pullback system (0.5 mm/s). All images underwent a randomized, double blind, offline volumetric reconstruction analysis (Volcano Image Analysis software V3.1) by an experienced evaluator. The quantitative volumetric analysis was completed in 20-mm segments from the ostium of the renal artery. The average vessel volume (mm^3) was computed by average vessel area (mm^2) ×20-mm segment. When plaques were identified, PV percentage (%PV) was calculated by (PV/average vessel volume) ×100. The change in %PV from the 3-months to 6-months was determined as delta %PV (D%PV).[33]

Aortic Distensibility—Cross-sectional MDCT images of the aorta were displayed with Analyze™, and 5 consecutive slices at both the systolic and diastolic phases traced. Subsequently, the average surface areas of aorta at systole and diastole were calculated, and its distensibility ($mmHg^{-1}$) assessed as: (maximum change in area/ (minimum area × (SBP-DBP)).[34]

Ex-vivo Studies

Micro-CT—After the kidney was flushed, microfil MV122 (an intravascular contrast agent) was perfused into the kidney under physiological pressure through a cannula ligated in the renal artery. Samples were prepared and scanned at 0.5° angular increments at 20-μm resolution. The spatial density of microvessels (diameters <500μm) in the renal cortex was calculated using Analyze™ and classified as small (20–40μm), medium (40–200μm), or large (200–500μm) microvessels.[35] Furthermore, the 3D nature of the micro-CT dataset allows calculations of vessel tortuosity, an index of vascular maturity. Specifically, the three-dimensional vascular path length (actual length) and linear length (the shortest distance from base to tip) were determined from the base of the main vessel at the corticomedullary junction to its tip at the superficial cortex. Tortuosity index was analyzed by dividing the path length by the linear length.[36]

Vascular Histology—Segments of vessels were dissected from comparable topographic locations in the abdominal aorta, renal artery and femoral artery of each animal, and 5-mm sections stained with H&E, trichrome, Sirius-Red, CD107a, E06, CD31, Von Kossa, α-SMA and Movat Pentachrome, and examined by light microscopy for the presence of atherosclerotic plaques. The media and lumen cross-sectional areas (CSA) of each vessel were traced (Analyze™), and their ratio in each vessel averaged for each group.[37] In addition, sections of the aorta were digitalized for histomorphometry of the lesions, including the lesion area and tunica media, using the Analyze™ analysis software. The normalized plaque area, expressed as the ratio of the lesion to medial areas, was used to adjust and compare arteries of different sizes.[38] Plaque area was calculated using slides stained for elastin and collagen.

Renal Histology—Kidney fibrosis was examined by Picro-sirius red, fat deposition by Oil-red-O, and oxidative stress by OX-LDL staining in 5-μm paraffin embedded mid-hilar renal cross-sections. The histochemical analysis utilized a computer-aided image-analysis program (AxioVision, Carl Zeiss MicroImaging, Thornwood, NY). Staining was semi-automatically quantified in 10–15 fields in each slide, expressed as the fraction of kidney surface area, and the results from all fields averaged. [22] In-situ renal production of superoxide anion was evaluated by fluorescence microscopy after DHE staining and apoptosis by TUNEL. Tubular injury was scored on a 1–5 scale (1:<10%, 2:10–25%, 3:26–50%, 4:51–75% and 5:>75% injury) in 40× H&E slides, based on tubular dilation, atrophy, cast formation, sloughing tubular cells, or basement membrane thickening.[39]

Renal arterial endothelial function—Renal artery segments were placed in Krebs solution, and sections (n=8/pig, 7 pigs/group) were mounted in individual organ chambers (one per renal artery ring), attached to an isometric force transducer with continuous recording, and contracted using potassium chloride (20mM).[40] Endothelium functionality was confirmed by the response to Acetylcholine (Ach) (1×10^{-6}M) and vessel rings allowed to equilibrate for 30 minutes. Following pre-contraction with endothelin-1 (10^{-7}M), incremental concentrations of Ach (10^{-9}–10^{-4}M) were administered to evaluate endothelium-dependent relaxation, and endothelium-independent-vasodilation with sodium nitroprusside (10^{-9}–10^{-4}M), respectively.

Statistical analysis

Statistical analysis was performed using JMP software package version 11.0 (SAS Institute, Cary, NC). Results were expressed as mean±SEM for normally distributed variables or median (range) for non-Gaussian distributed data. Comparisons within groups were performed using ANOVA followed by paired Student's t-test and among groups using unpaired t-test or non-parametric (Wilcoxon followed by Kruskal-Wallis) tests when appropriate. $P \leq 0.05$ was considered statistically significant

Results

Table 1 shows the characteristics of the animals included in the study. All groups significantly increased body weight at 6 months, with WT-AD being the heaviest. Body weight was lower in GOF compared to WT pigs, likely because they were the first generation after cloning. MAP was increased in both GOF groups at 3- and 6-months, but not in WT-AD. SVR, total serum cholesterol, LDL-C, VLDL-C, and triglycerides levels also rose in GOF-ND and GOF-AD compared with WT, whereas HDL-C was elevated only in GOF-AD at 6-months. LDL-C level at 3-months was 12-fold and 24-fold higher in PCSK9-ND and PCSK9-AD, respectively, compared to WT, and 13-fold and 29 times higher at 6-months ($p<0.05$). Albumin/creatinine ratio remained unchanged among the groups. The levels of PCSK9 after a 6-month diet were similarly elevated in the GOF-ND and GOF-AD compared to the WT-ND and WT-AD ($p<0.05$, Table 1), confirming the success of the mutation. Notably, LDL-C and PCSK9 levels correlated well (Figure 1E). Triglyceride levels were nearly 2-fold higher in PCSK9 groups compared to WT, at 3-months and 6-months. In WT-AD, lipid levels were elevated compared to WT-ND, but total and LDL-C

remained markedly lower than in GOF-ND, although their triglyceride and VLDL-C levels were higher.

Table 2 shows a summary of the directional changes in parameters in GOF compared to WT-ND pigs during the course of the diet.

Renal Vascular Studies

Average renal artery diameter in-vivo by CTA was smaller in both GOF groups compared to WT-ND at both the 3-months and 6-months studies (Figure 1A). In-vivo IVUS data are presented in Figure 1B. Vessel volume and PV at 3 months tended to be higher in GOF-AD compared to GOF-ND and WT, but only vessel volume at 6-months was significantly higher than in GOF-ND Both GOF groups showed a significant increase in renal artery PV from 3- to 6-months of diet, with no change over time in vessel volume or %PV. At 6 months, arterial wall thickening (increased media-to-lumen ratio) was evident ex-vivo in the renal artery in GOF-AD. Furthermore, neointimal hyperplasia was evident in the renal artery in GOF-AD, but not in WT and GOF-ND. GOF-AD demonstrated a more diffuse intima-media thickening in the renal artery compared to GOF-ND and WT (Figure 1C). The isolated renal artery vasorelaxation response to Ach was attenuated in GOF-AD but not in GOF-ND, while the response to SNP was unchanged (Figure 1D).

Renal Hemodynamics, Function and Oxygenation

Single-kidney cortical and medullary perfusion, RBF, and GFR were not different among the groups at either time point (Table 1). Renal cortical and medullary R_2* was higher in GOF-AD compared with WT and GOF-ND at 3-months, but became elevated in both groups at 6-months, suggesting decreased oxygenation in transgenic PCSK9 groups (Figure 2A). MRE showed no difference in medullary stiffness among the groups at 3-months, but an increase in both GOF groups by 6-months (Figure 2B). The spatial density of small, medium and large-sized cortical microvessels was increased in both GOF groups, whereas microvascular tortuosity was unchanged (Figure 2C).

Picro-sirius red staining showed significantly greater cortical and medullary fibrosis in the GOF groups compared with WT (Figure 3A), and tubular injury score was increased (Table 1). Oil-Red-O staining showed greater fat accumulations in GOF-AD compared with WT and GOF-ND, while E06 increased in both GOF groups (Figure 3B). DHE staining, an index of tissue oxidative stress, was also elevated in both GOF groups compared to WT (Figure 3C), and the TUNEL assay revealed a significant increase in the number of apoptotic cells (Figure 3D).

Aortic Studies

Aortic distensibility, a CT-derived parameter of early structural wall changes, remained unchanged at 3 months but significantly decreased in GOF-AD compared to WT and GOF-ND (Figure 4A) at 6-months. The sites of ex-vivo vascular sample collection are illustrated in Figure 4. Arterial wall thickening was observed ex-vivo in the GOF aorta at 6 months. Furthermore, the aorta showed eccentric fibrofatty plaque with intimal thickening and fatty streaks in GOF groups, while WT showed unremarkable morphology (Figure 4B). GOF-AD

demonstrated a more diffuse intima-media thickening in the aorta compared to GOF-ND and WT. However, while the normalized lesion area in the inferior aorta appeared to be slightly increased in GOF groups by histomorphometry, this has not reached statistical significance levels (Figure 4D).

Femoral Artery Studies

At 6 months, arterial wall thickening was evident ex-vivo in the femoral artery. In addition, the femoral artery showed eccentric fibrofatty plaque with intimal thickening and fatty streaks in both GOF groups, but not in WT (Figure 5). The lesions in WT animals were consistent with minimal to mild neointimal thickening, consisting mainly of smooth muscle cells and proteoglycans and rare foam cells, whereas GOF-ND and GOF AD generally showed minimal to mild fibrofatty or fibroatheromatous plaques accompanied by necrosis with an overlying fibrous cap, and complications of intimal calcification (speckled to dense).

DISCUSSION

Our study demonstrates that PCSK9-GOF in Ossabaw mini-pigs induces peripheral arterial disease involving the renal artery, femoral artery, and aorta, which is exacerbated by superimposition of an atherogenic diet. This is reflected in development of early atherosclerotic plaques in the peripheral vessels, aortic stiffening, and development of hypertension. In the kidney, we observed intra-renal fat deposition, increased oxidative stress, apoptosis, hypoxia, endothelial dysfunction and mild fibrosis, which are consistent with the effects of early atherosclerosis and hypercholesterolemia on renal injury. Therefore, this study suggests that PCSK9-GOF model may be useful as a preclinical platform to study atherosclerotic peripheral artery disease.

An important hurdle to current studies of atherogenesis is the lack of large animal models to investigate the progression and mechanisms of the disease process. The mouse, hamster, rat, and rabbit models are useful animal models of atherosclerosis,[4, 5, 41] yet pigs show many genetic, anatomical and physiological similarities to humans, which allow using clinically-applicable medical devices and treatments, and collecting sufficient blood and tissue samples for analysis.

Several breeds of swine are widely used for pre-clinical evaluation of safety and efficacy of medical interventions. Previous studies have shown that transgenic Yucatan mini-pigs expressing human, liver-specific D374Y-PCSK9 and fed an atherogenic diet for approximately 1 year, demonstrated increased cholesterol (to 772mg/dL) and LDL-C (to 425 mg/dL) level.[18] Similarly, cholesterol levels increase in diabetic/hypercholesterolemic, Rapacz familial hypercholesterolemic, domestic, Ossabaw, and LDLR knockout domestic and Yucatan pig models, but to lower levels than those achieved in this model after a 3-months diet. [42–45] Some pig models are limited by a big body size, difficulty of triggering atherosclerotic lesions, or a prolonged induction period. Accelerating atherosclerosis in healthy pigs is difficult,[46, 47] and often necessitates feeding with high fat or other atherosclerosis-accelerating procedures, such as balloon injury or streptozotocin-induced diabetes.[48–50] Additional drawbacks of some pig models might be a broad genetic background and the nature of the mutation, as well as the diversity secondary to the efforts

to miniaturize the pig by crossing with smaller pig breeds. The balloon injury intervention, while useful, has yet to fully mimic the natural occurrence of atherosclerosis and realistic response to applied treatments and devices. The occurrence of atherosclerosis following balloon injury has yet to be evaluated in the Ossabaw PCSK9-GOF model.

PCSK9, a member of the proprotein convertase family, is a secretory protein that regulates LDLR after transcription, primarily via degradation of the hepatic LDLR. PCSK9 is expressed in the liver and to a lesser extent in the intestine, kidneys,[51] as well as in human atherosclerotic plaques. PCSK9 binds hepatic LDLRs directing them to lysosomal degradation, and is a crucial regulator of LDL-C levels.[52] Human D374Y-PCSK9 binds the porcine LDLR with high affinity.[53] The GOF D374Y upturns affinity of this binding, which causes a severe form of autosomal dominant hypercholesterolemia in humans.[54] The LDLR residues demonstrated to be critical for binding of human D374Y-PCSK9.[55] Previous studies have shown that the pathologic effect of PCSK9-GOF occurs primarily through an increase in the level of LDL-C [18], but it may also have a local effect in the vascular wall, which may be independent of its effect on systemic cholesterol levels.[56, 57] Its effect on triglyceride and HDL-C levels is more modest, and is somewhat independent of LDLR. For example, PCSK9 enhances intestinal overproduction of triglyceride-rich lipoproteins through both LDLR-dependent and -independent mechanisms. [14, 54, 58]

One of the novel aspects of our model is the imposition of a PCSK9-GOF mutation on the genetic background of Ossabaw minipigs. Consequent to natural selection, WT Ossabaw pigs are inherently prone to dyslipidemia and mild atherosclerotic lesions, especially when fed a high-fat diet, but their development may take months.[19]Our study demonstrates that a PCSK9-GOF mutation in Ossabaw pig produces a promising model for translational vascular research. Ossabaw PCSK9-GOF pigs have a compact body size, a well-characterized background, and lesion formation within a relatively short time. In the current study, we found that ectopic expression of PCSK9-D374Y in Ossabaw pigs significantly elevated systemic levels of PCSK9. The elevated levels of PCSK9 in the GOF-ND group in the face of low levels in WT-AD pigs are consistent with rise in PCSK9 resulting from the mutation, rather than from the AD alone. Indeed, PCSK9-GOF in pigs fed ND markedly aggravated dyslipidemia compared to WT pigs fed AD, although the higher triglycerides and VLDL-C levels in WT-AD remain to be clarified.

Furthermore, PCSK9-GOF induced kidney vascular remodeling as early as 3-months after initiation of ND (6 months of age). Superimposition of AD exacerbated development of early atherosclerosis lesions in peripheral arteries, renal arterial remodeling, endothelial dysfunction, and aortic stiffness, possibly due to almost doubling of serum cholesterol levels. These findings suggest that the predominant effect of PCSK9-GOF mutation on peripheral vascular disease and target organ injury in this model are attainable without, but can be markedly amplified by, a high-fat diet. Interestingly, we observed an increase in blood pressure in both GOF groups. This might be due to higher SVR secondary to vascular remodeling and vasoconstriction imposed by elevated cholesterol levels, but also to possible involvement of some PCSK9 variants in regulation of blood pressure,[59] as well as the sympathetic nervous system hyperactivity.[60] The observation that blood pressure was

elevated in GOF-ND and GOF-AD, but not in WT-AD pigs, supports the role of PCSK9 and elevated cholesterol levels in development of hypertension in our model.

The mechanism underlying vascular remodeling (wall thickening, plaque development, changes in microvascular architecture, etc.) in our model likely involves an increase in plasma and tissue LDL-C concentration, which may in turn decrease release of nitric oxide and accelerate endothelial apoptosis and dysfunction, vascular smooth muscle cells proliferation, as well as formation of atherosclerotic plaques.[61] Indeed, we observed in GOF groups an increase in media-to-lumen ratio in peripheral vessels with early plaques and intimal thickening. Yet, a slight increase in the plaque area in the GOF groups by histomorphometry has not reached statistical significance levels due to high variability, possibly because subjective elements in histomorphometry measurements might be accentuated in mild atherosclerotic lesions.[62]

We also observed endothelial dysfunction only in the GOF-AD renal artery, indicating acceleration of vascular dysfunction by the high-fat diet. Possibly, a certain threshold of levels (and likely also duration) of hypercholesterolemia may account for the magnified effect on renal arterial endothelial function in GOF-AD. Yet, both GOF groups developed ex-vivo positive remodeling of peripheral vessels, a common feature of human-like atherosclerotic lesions that can reduce the elasticity of the artery walls and are commonly initiated by endothelial injury and dysfunction.[63] While organ bath studies were not performed on other vessels, aortic distensibility was also significantly decreased in GOF-AD, indicating the impact of the diet.

The aorta and femoral artery showed eccentric fibrofatty plaque with intimal thickening and fatty streaks, whereas the atherosclerotic structural changes in the renal artery were milder, and consisted mainly of arterial wall thickening. Presumably, the renal artery might be less susceptible to the functional and structural effects of AD, and changes take longer to become measurable. IVUS studies in the renal artery showed a rise in PV in both GOF groups over the course of the study. Compared with 3-months data, the 6-months %PV and vessel volume appeared to be slightly increased (albeit not significantly), while the significantly increased PV likely reflects initiation of positive remodeling and progression of atherosclerosis, which may have contributed to the increases in arterial stiffness and blood pressure. Yet, the difference in %PV and PV by IVUS was not significantly different between WT and GOF-ND. Indeed, because the Ossabaw pig strain is prone to spontaneous vascular pathology, the WT pigs showed mild renal artery remodeling; very high cholesterol levels, as those achieved in GOF-AD, may be required to increase vascular remodeling even further.

Most of the renal arteries in GOF pigs, particularly GOF-AD, were characterized by medial hypertrophy, possibly partly due to the mild hypertension that both GOF groups developed. Medial area in IVUS analysis is often included in the “plaque area” measurements, which are derived by subtracting the lumen area from external elastic membrane area (Figure 1). This approach results in a slight overestimation of atheroma area (in comparison to histology) by including the media, and may have led to a slight discrepancy between IVUS and histology.[64] The functional significance of aortic remodeling is underscored by its

decreased elasticity, a common pathologic mechanism that results in development and progression of vascular disease and hypertension.

The elevated renal DHE and TUNEL staining in the GOF groups indicate renal oxidative stress and apoptosis, respectively, possibly due to accumulation of ox-LDL and development of endothelial dysfunction, which may, in turn, lead to kidney hypoxia and tubular injury. Notably, E06 staining may react with apoptotic cells and may reflect the degree of apoptosis, rather than ox-LDL levels.[65] Given that PCSK9 promotes ox-LDL-induced apoptosis.[66] As we have shown before in models of hypercholesterolemia,[67] we observed microvascular remodeling reflected in an increase in the cortical vascular density in GOF pigs, probably due to oxidative stress and inflammation. As opposed to arterial lesions, microvascular density was similarly increased in both GOF group, suggesting that alterations in microvascular architecture precede or require a lower cholesterol levels than macrovascular remodeling. Newly formed microvessels sustain cortical and medullary perfusion and function in this noxious milieu. Nevertheless, increased oxidative stress and inefficient oxygen utilization may result in hypoxia and fibrosis.[68] Interestingly, these changes were similar in GOF-ND and GOF-AD groups suggesting that cholesterol levels prevailing in this model when fed a standard diet suffice to induce subtle renal injury.

Limitations

The study is limited by use of relatively young animals and short diet duration, yet this model recapitulates many features of atherosclerosis in humans. The Ossabaw pig strain that constitutes our WT group is naturally prone to development of vascular lesions, which likely attenuated observed differences among the groups. As a result, differences by IVUS and by histology were modest in the PCSK9 GOF groups compared to WT. Interestingly, we also observed subtle differences between the GOF-ND and GOF-AD groups, perhaps due to short duration of diet, implying that an atherogenic diet is not mandatory to produce some features of early atherosclerosis in this model, although it does aggravate them. Unaltered kidney function, normal albumin/creatinine ratio, and mild tubular injury, imply a relatively minor damage to the kidney parenchyma. Furthermore, longer observation periods or injury may be needed to detect obstructive atherosclerotic lesions and deterioration in renal function. Most of the effects of PCSK9 are likely mediated via LDLR in the liver; we cannot rule out the possibility of a minor direct effect in our study.

While we attempted to be consistent in sample collection sites, there might have been some variability among animals; hence, we normalized media to luminal CSA. Furthermore, sampling 5 μm slides ex-vivo (histology) vs. 2 cm (IVUS) or the entire renal artery (CTA) may have contributed to slightly different observations made using these modalities.

Conclusion

In the current study, we observed in a novel Ossabaw D374Y PCSK9-GOF model prominent hypercholesterolemia, renal arterial endothelial dysfunction, peripheral vascular remodeling, and spontaneous development of early atherosclerotic lesions by the time the pigs reached 9-months of age. We also found clear evidence of early kidney injury, although its function remained intact. This model, therefore, shows many similarities to human peripheral artery

disease and may provide a useful tool for translational research and to assess atherosclerotic features and management.

Acknowledgments

Supported by funding from Recombinetics® Inc. All of the authors have read the authorship agreement and are in compliance with it.

Dr. Daniel F. Carlson is employed by Recombinetics, Inc. Dr. Lilach O. Lerman reports grants from Recombinetics, Inc., during the conduct of the study; grants from Stealth Biopharmaceutical, and personal fees from Novartis, outside the submitted work; In addition, Dr. Lerman has a patent on Humanin in atherosclerosis issued.

Abbreviations

GOF	gain-of-function
PCSK9	proprotein convertase subtilisin/kexin type-9
WT	wild-type
AD	atherogenic diet
MDCT	multidetector computed-tomography
LDL-C	low-density lipoprotein-cholesterol
ND	normal diet
IVUS	intravascular ultrasound
BOLD-MRI	blood oxygen level-dependent magnetic resonance imaging
TUNEL	Terminal deoxynucleotidyl transferase dUTP nick-end labeling
DHE	dihydroethidium
MAP	mean arterial pressure
HDL-C	high-density lipoprotein-cholesterol
ROI	region of interest
RBF	renal blood flow
GFR	glomerular filtration rate
CTA	computed tomography angiography
MPR	multiplanar-reformatted
MRE	magnetic resonance elastography
VLDL-C	Very low-density lipoprotein cholesterol

References

1. Lusis AJ. Atherosclerosis. Nature. 2000; 407:233–41. [PubMed: 11001066]
2. Celermajer DS, Chow CK, Marijon E, Anstey NM, Woo KS. Cardiovascular disease in the developing world: prevalences, patterns, and the potential of early disease detection. J Am Coll Cardiol. 2012; 60:1207–16. [PubMed: 22858388]
3. Sillesen H, Falk E. Why not screen for subclinical atherosclerosis? Lancet. 2011; 378:645–6. [PubMed: 21440933]
4. Breslow JL. Mouse models of atherosclerosis. Science. 1996; 272:685–8. [PubMed: 8614828]
5. Mohler ER 3rd, Sarov-Blat L, Shi Y, Hamamdzic D, Zalewski A, Macphee C, et al. Site-specific atherogenic gene expression correlates with subsequent variable lesion development in coronary and peripheral vasculature. Arterioscler Thromb Vasc Biol. 2008; 28:850–5. [PubMed: 18276914]
6. Skold BH, Getty R, Ramsey FK. Spontaneous atherosclerosis in the arterial system of aging swine. Am J Vet Res. 1966; 27:257–73. [PubMed: 4161799]
7. Reiser R, Sorrels MF, Williams MC. Influence of high levels of dietary fats and cholesterol on atherosclerosis and lipid distribution in swine. Circ Res. 1959; 7:833–46. [PubMed: 14437214]
8. Getz GS, Reardon CA. Animal models of atherosclerosis. Arterioscler Thromb Vasc Biol. 2012; 32:1104–15. [PubMed: 22383700]
9. Strom TB, Tveten K, Leren TP. PCSK9 acts as a chaperone for the LDL receptor in the endoplasmic reticulum. Biochem J. 2014; 457:99–105. [PubMed: 24144304]
10. Timms KM, Wagner S, Samuels ME, Forbey K, Goldfine H, Jammulapati S, et al. A mutation in PCSK9 causing autosomal-dominant hypercholesterolemia in a Utah pedigree. Hum Genet. 2004; 114:349–53. [PubMed: 14727179]
11. Cohen JC, Boerwinkle E, Mosley TH Jr, Hobbs HH. Sequence variations in PCSK9, low LDL, and protection against coronary heart disease. N Engl J Med. 2006; 354:1264–72. [PubMed: 16554528]
12. Gauthier B, Robb M, Gaudet F, Ginsburg GS, McPherson R. Characterization of a cholesterol response element (CRE) in the promoter of the cholesteryl ester transfer protein gene: functional role of the transcription factors SREBP-1a, −2, and YY1. J Lipid Res. 1999; 40:1284–93. [PubMed: 10393213]
13. Jeong HJ, Lee HS, Kim KS, Kim YK, Yoon D, Park SW. Sterol-dependent regulation of proprotein convertase subtilisin/kexin type 9 expression by sterol-regulatory element binding protein-2. J Lipid Res. 2008; 49:399–409. [PubMed: 17921436]
14. Kwakernaak AJ, Lambert G, Dullaart RP. Plasma proprotein convertase subtilisin-kexin type 9 is predominantly related to intermediate density lipoproteins. Clin Biochem. 2014; 47:679–82. [PubMed: 24680982]
15. Druce I, Abujrad H, Ooi TC. PCSK9 and triglyceride-rich lipoprotein metabolism. J Biomed Res. 2015; 29
16. Dai Y, Vaught TD, Boone J, Chen SH, Phelps CJ, Ball S, et al. Targeted disruption of the alpha1,3-galactosyltransferase gene in cloned pigs. Nat Biotechnol. 2002; 20:251–5. [PubMed: 11875425]
17. Lai L, Kolber-Simonds D, Park KW, Cheong HT, Greenstein JL, Im GS, et al. Production of alpha-1,3-galactosyltransferase knockout pigs by nuclear transfer cloning. Science. 2002; 295:1089–92. [PubMed: 11778012]
18. Al-Mashhadi RH, Sorensen CB, Kragh PM, Christoffersen C, Mortensen MB, Tolbod LP, et al. Familial hypercholesterolemia and atherosclerosis in cloned minipigs created by DNA transposition of a human PCSK9 gain-of-function mutant. Sci Transl Med. 2013; 5:166ra1.
19. Dyson MC, Alloosh M, Vuchetich JP, Mokelke EA, Sturek M. Components of metabolic syndrome and coronary artery disease in female Ossabaw swine fed excess atherogenic diet. Comp Med. 2006; 56:35–45. [PubMed: 16521858]
20. Uzu T, Takeji M, Yamada N, Fujii T, Yamauchi A, Takishita S, et al. Prevalence and outcome of renal artery stenosis in atherosclerotic patients with renal dysfunction. Hypertens Res. 2002; 25:537–42. [PubMed: 12358138]

21. Textor SC. Ischemic nephropathy: where are we now? J Am Soc Nephrol. 2004; 15:1974–82. [PubMed: 15284283]
22. Eirin A, Zhu XY, Krier JD, Tang H, Jordan KL, Grande JP, et al. Adipose tissue-derived mesenchymal stem cells improve revascularization outcomes to restore renal function in swine atherosclerotic renal artery stenosis. Stem Cells. 2012; 30:1030–41. [PubMed: 22290832]
23. Perona JS, Ruiz-Gutierrez V. Quantification of major lipid classes in human triacylglycerol-rich lipoproteins by high-performance liquid chromatography with evaporative light-scattering detection. J Sep Sci. 2004; 27:653–9. [PubMed: 15387459]
24. Carlson DF, Garbe JR, Tan W, Martin MJ, Dobrinsky JR, Hackett PB, et al. Strategies for selection marker-free swine transgenesis using the Sleeping Beauty transposon system. Transgenic Res. 2011; 20:1125–37. [PubMed: 21221779]
25. Kramer MG, Barajas M, Razquin N, Berraondo P, Rodrigo M, Wu C, et al. In vitro and in vivo comparative study of chimeric liver-specific promoters. Molecular therapy : the journal of the American Society of Gene Therapy. 2003; 7:375–85. [PubMed: 12668133]
26. Ebrahimi B, Gloviczki M, Woollard JR, Crane JA, Textor SC, Lerman LO. Compartmental analysis of renal BOLD MRI data: introduction and validation. Invest Radiol. 2012; 47:175–82. [PubMed: 22183077]
27. Warner L, Glockner JF, Woollard J, Textor SC, Romero JC, Lerman LO. Determinations of renal cortical and medullary oxygenation using blood oxygen level-dependent magnetic resonance imaging and selective diuretics. Invest Radiol. 2011; 46:41–7. [PubMed: 20856128]
28. Daghini E, Primak AN, Chade AR, Krier JD, Zhu XY, Ritman EL, et al. Assessment of renal hemodynamics and function in pigs with 64-section multidetector CT: comparison with electron-beam CT. Radiology. 2007; 243:405–12. [PubMed: 17456868]
29. Chade AR, Rodriguez-Porcel M, Grande JP, Krier JD, Lerman A, Romero JC, et al. Distinct renal injury in early atherosclerosis and renovascular disease. Circulation. 2002; 106:1165–71. [PubMed: 12196346]
30. Krier JD, Crane JA, Eirin A, Zhu XY, Lerman A, Lerman LO. Hemodynamic determinants of perivascular collateral development in swine renal artery stenosis. Am J Hypertens. 2013; 26:209–17. [PubMed: 23382405]
31. Boogers MJ, Schuijf JD, Kitslaar PH, van Werkhoven JM, de Graaf FR, Boersma E, et al. Automated quantification of stenosis severity on 64-slice CT: a comparison with quantitative coronary angiography. JACC Cardiovasc Imaging. 2010; 3:699–709. [PubMed: 20633847]
32. Korsmo MJ, Ebrahimi B, Eirin A, Woollard JR, Krier JD, Crane JA, et al. Magnetic resonance elastography noninvasively detects in vivo renal medullary fibrosis secondary to swine renal artery stenosis. Invest Radiol. 2013; 48:61–8. [PubMed: 23262789]
33. Park KH, Kwon TG, Matsuzawa Y, Sun T, Liu Z, Lennon RJ, et al. Association between the vasa vasorum and the atherosclerotic changes in cardiac allograft vasculopathy: volumetric analysis. Eur Heart J Cardiovasc Imaging. 2016; 17:272–9. [PubMed: 26657475]
34. Liu CY, Chen D, Bluemke DA, Wu CO, Teixido-Tura G, Chugh A, et al. Evolution of aortic wall thickness and stiffness with atherosclerosis: long-term follow up from the multi-ethnic study of atherosclerosis. Hypertension. 2015; 65:1015–9. [PubMed: 25776078]
35. Zhu XY, Chade AR, Rodriguez-Porcel M, Bentley MD, Ritman EL, Lerman A, et al. Cortical microvascular remodeling in the stenotic kidney: role of increased oxidative stress. Arterioscler Thromb Vasc Biol. 2004; 24:1854–9. [PubMed: 15308558]
36. Chade AR, Bentley MD, Zhu X, Rodriguez-Porcel M, Niemeyer S, Amores-Arriaga B, et al. Antioxidant intervention prevents renal neovascularization in hypercholesterolemic pigs. J Am Soc Nephrol. 2004; 15:1816–25. [PubMed: 15213269]
37. Jones ES, Black MJ, Widdop RE. Influence of Angiotensin II Subtype 2 Receptor (AT(2)R) Antagonist, PD123319, on Cardiovascular Remodelling of Aged Spontaneously Hypertensive Rats during Chronic Angiotensin II Subtype 1 Receptor (AT(1)R) Blockade. Int J Hypertens. 2012; 2012:543062. [PubMed: 22500216]
38. Fenning RS, Burgert ME, Hamamdzic D, Peyster EG, Mohler ER, Kangovi S, et al. Atherosclerotic plaque inflammation varies between vascular sites and correlates with response to inhibition of lipoprotein-associated phospholipase A2. J Am Heart Assoc. 2015; 4

39. Eirin A, Li Z, Zhang X, Krier JD, Woollard JR, Zhu XY, et al. A mitochondrial permeability transition pore inhibitor improves renal outcomes after revascularization in experimental atherosclerotic renal artery stenosis. Hypertension. 2012; 60:1242–9. [PubMed: 23045468]
40. Eirin A, Ebrahimi B, Zhang X, Zhu XY, Woollard JR, He Q, et al. Mitochondrial protection restores renal function in swine atherosclerotic renovascular disease. Cardiovasc Res. 2014; 103:461–72. [PubMed: 24947415]
41. Koskinas KC, Feldman CL, Chatzizisis YS, Coskun AU, Jonas M, Maynard C, et al. Natural history of experimental coronary atherosclerosis and vascular remodeling in relation to endothelial shear stress: a serial, in vivo intravascular ultrasound study. Circulation. 2010; 121:2092–101. [PubMed: 20439786]
42. Hamamdzic D, Wilensky RL. Porcine models of accelerated coronary atherosclerosis: role of diabetes mellitus and hypercholesterolemia. J Diabetes Res. 2013; 2013:761415. [PubMed: 23844374]
43. Artinger S, Deiner C, Loddenkemper C, Schwimmbeck PL, Schultheiss HP, Pels K. Complex porcine model of atherosclerosis: induction of early coronary lesions after long-term hyperlipidemia without sustained hyperglycemia. Can J Cardiol. 2009; 25:e109–14. [PubMed: 19340354]
44. Li Y, Fuchimoto D, Sudo M, Haruta H, Lin QF, Takayama T, et al. Development of HumanLike Advanced Coronary Plaques in Low-Density Lipoprotein Receptor Knockout Pigs and Justification for Statin Treatment Before Formation of Atherosclerotic Plaques. J Am Heart Assoc. 2016; 5
45. Davis BT, Wang XJ, Rohret JA, Struzynski JT, Merricks EP, Bellinger DA, et al. Targeted disruption of LDLR causes hypercholesterolemia and atherosclerosis in Yucatan miniature pigs. PLoS One. 2014; 9:e93457. [PubMed: 24691380]
46. Prescott MF, McBride CH, Hasler-Rapacz J, Von Linden J, Rapacz J. Development of complex atherosclerotic lesions in pigs with inherited hyper-LDL cholesterolemia bearing mutant alleles for apolipoprotein B. Am J Pathol. 1991; 139:139–47. [PubMed: 1853929]
47. Prescott MF, Hasler-Rapacz J, von Linden-Reed J, Rapacz J. Familial hypercholesterolemia associated with coronary atherosclerosis in swine bearing different alleles for apolipoprotein B. Ann N Y Acad Sci. 1995; 748:283–92. discussion 92–3. [PubMed: 7695172]
48. Granada JF, Kaluza GL, Wilensky RL, Biedermann BC, Schwartz RS, Falk E. Porcine models of coronary atherosclerosis and vulnerable plaque for imaging and interventional research. EuroIntervention. 2009; 5:140–8. [PubMed: 19577996]
49. Thim T, Hagensen MK, Drouet L, Bal Dit Sollier C, Bonneau M, Granada JF, et al. Familial hypercholesterolaemic downsized pig with human-like coronary atherosclerosis: a model for preclinical studies. EuroIntervention. 2010; 6:261–8. [PubMed: 20562079]
50. Wilensky RL, Shi Y, Mohler ER 3rd, Hamamdzic D, Burgert ME, Li J, et al. Inhibition of lipoprotein-associated phospholipase A2 reduces complex coronary atherosclerotic plaque development. Nat Med. 2008; 14:1059–66. [PubMed: 18806801]
51. Attie AD, Seidah NG. Dual regulation of the LDL receptor--some clarity and new questions. Cell Metab. 2005; 1:290–2. [PubMed: 16054075]
52. Mousavi SA, Berge KE, Leren TP. The unique role of proprotein convertase subtilisin/kexin 9 in cholesterol homeostasis. J Intern Med. 2009; 266:507–19. [PubMed: 19930098]
53. Al-Mashhadi RH, Sorensen CB, Kragh PM, Christoffersen C, Mortensen MB, Tolbod LP, et al. Familial hypercholesterolemia and atherosclerosis in cloned minipigs created by DNA transposition of a human PCSK9 gain-of-function mutant. Sci Transl Med. 2013; 5:166ra1.
54. Soutar AK. Unexpected roles for PCSK9 in lipid metabolism. Curr Opin Lipidol. 2011; 22:192–6. [PubMed: 21494143]
55. Zhang DW, Lagace TA, Garuti R, Zhao Z, McDonald M, Horton JD, et al. Binding of proprotein convertase subtilisin/kexin type 9 to epidermal growth factor-like repeat A of low density lipoprotein receptor decreases receptor recycling and increases degradation. J Biol Chem. 2007; 282:18602–12. [PubMed: 17452316]
56. Giunzioni I, Tavori H, Covarrubias R, Major AS, Ding L, Zhang Y, et al. Local effects of human PCSK9 on the atherosclerotic lesion. J Pathol. 2016; 238:52–62. [PubMed: 26333678]

57. Tavori H, Giunzioni I, Predazzi IM, Plubell D, Shivinsky A, Miles J, et al. Human PCSK9 promotes hepatic lipogenesis and atherosclerosis development via apoE- and LDLR-mediated mechanisms. Cardiovasc Res. 2016; 110:268–78. [PubMed: 26980204]
58. Rashid S, Tavori H, Brown PE, Linton MF, He J, Giunzioni I, et al. Proprotein convertase subtilisin kexin type 9 promotes intestinal overproduction of triglyceride-rich apolipoprotein B lipoproteins through both low-density lipoprotein receptor-dependent and -independent mechanisms. Circulation. 2014; 130:431–41. [PubMed: 25070550]
59. Tran NT, Aslibekyan S, Tiwari HK, Zhi D, Sung YJ, Hunt SC, et al. PCSK9 variation and association with blood pressure in African Americans: preliminary findings from the HyperGEN and REGARDS studies. Front Genet. 2015; 6:136. [PubMed: 25904937]
60. da Silva AA, do Carmo J, Dubinion J, Hall JE. The role of the sympathetic nervous system in obesity-related hypertension. Curr Hypertens Rep. 2009; 11:206–11. [PubMed: 19442330]
61. Vanhoutte PM, Shimokawa H, Tang EH, Feletou M. Endothelial dysfunction and vascular disease. Acta Physiol (Oxf). 2009; 196:193–222. [PubMed: 19220204]
62. Wright CD, Vedi S, Garrahan NJ, Stanton M, Duffy SW, Compston JE. Combined inter-observer and inter-method variation in bone histomorphometry. Bone. 1992; 13:205–8. [PubMed: 1637566]
63. Brodsky SV, Yamamoto T, Tada T, Kim B, Chen J, Kajiya F, et al. Endothelial dysfunction in ischemic acute renal failure: rescue by transplanted endothelial cells. Am J Physiol Renal Physiol. 2002; 282:F1140–9. [PubMed: 11997331]
64. Tuzcu EM, Bayturan O, Kapadia S. Invasive imaging: Coronary intravascular ultrasound: a closer view. Heart. 2010; 96:1318–24. [PubMed: 20659952]
65. Panini SR, Yang L, Rusinol AE, Sinensky MS, Bonventre JV, Leslie CC. Arachidonate metabolism and the signaling pathway of induction of apoptosis by oxidized LDL/oxysterol. J Lipid Res. 2001; 42:1678–86. [PubMed: 11590225]
66. Liu LS, Bai XQ, Gao Y, Wu Q, Ren Z, Li Q, et al. PCSK9 Promotes oxLDL-Induced PC12 Cell Apoptosis Through the Bcl-2/Bax-Caspase 9/3 Signaling Pathway. J Alzheimers Dis. 2017
67. Chade AR, Krier JD, Galili O, Lerman A, Lerman LO. Role of renal cortical neovascularization in experimental hypercholesterolemia. Hypertension. 2007; 50:729–36. [PubMed: 17635852]
68. Lerman LO, Textor SC, Grande JP. Mechanisms of tissue injury in renal artery stenosis: ischemia and beyond. Prog Cardiovasc Dis. 2009; 52:196–203. [PubMed: 19917330]

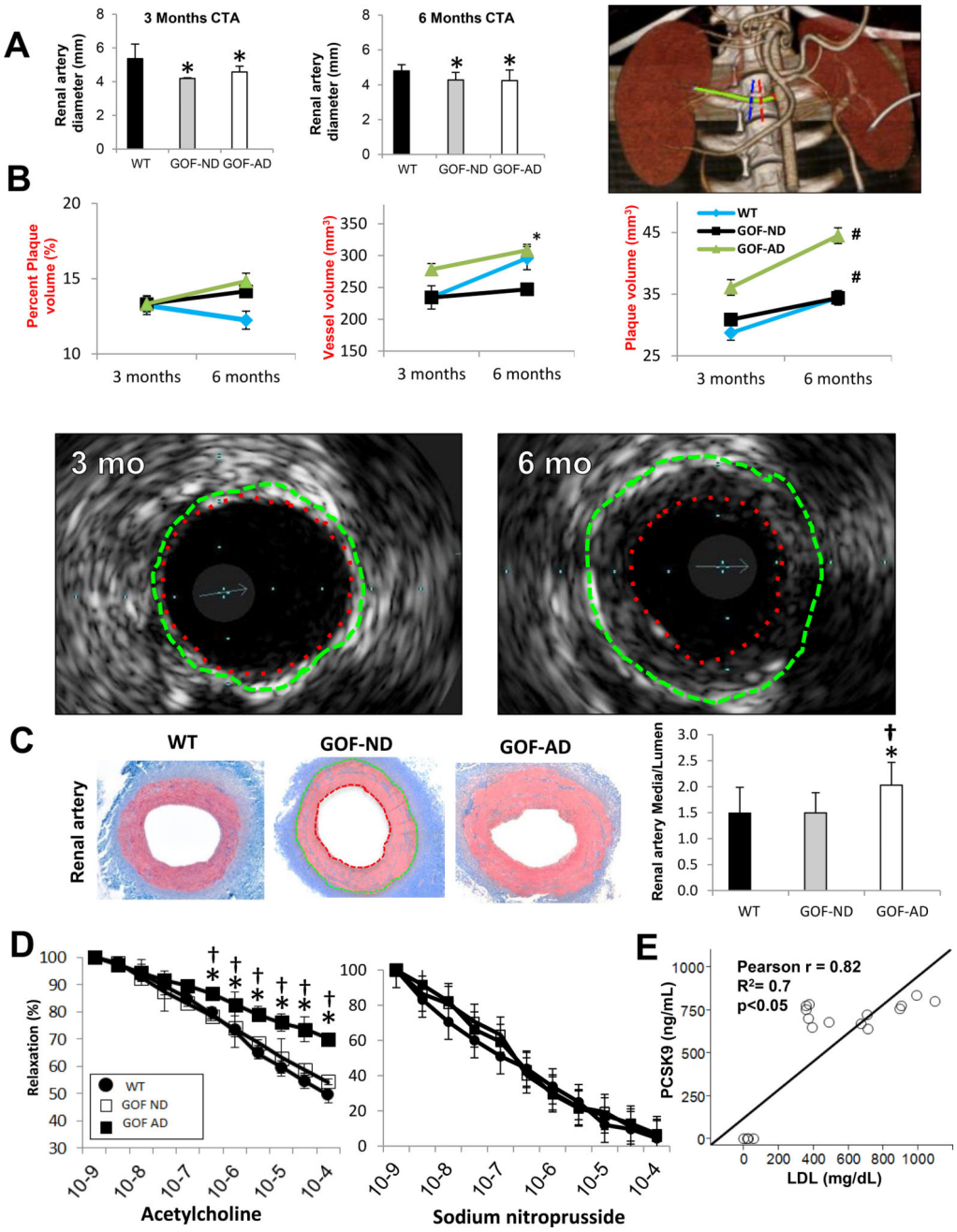

Figure 1.

(**A**) Representative computed tomography angiography (CTA) of the renal artery (green), showing proximal (red) and distal (blue) markings of a 5mm renal artery segment, and quantification showing a consistent decrease in the diameter of the renal artery, suggesting diffuse narrowing (n=7/group). (**B**) Intravascular ultrasound (IVUS) images obtained in a PCSK9 GOF-AD pig after 3 versus 6 months of diet, and their quantification in the groups. The images show the vessel wall (green dashed line: external elastic lamina) and lumen (red dashed line) areas. The area enclosed between them illustrates diffuse concentric neointimal hyperplasia at 6 compared to 3 months. (**C**) The renal artery in GOF-AD showed an increase

in media thickness (enclosed between the green and red outlines) relative to the lumen area (n=7/group). (**D**) Endothelial-dependent (left) and independent (right) relaxation responses to acetylcholine of renal arterial segments from Wild-type (WT) and GOF pigs, showing impaired relaxation response in GOF-AD (n=7/group). (**E**) LDL-C and PCSK9 levels showed a direct correlation. *p<0.05 vs. WT; #p<0.05 vs. 3mo; †p<0.05 vs. GOF-ND.

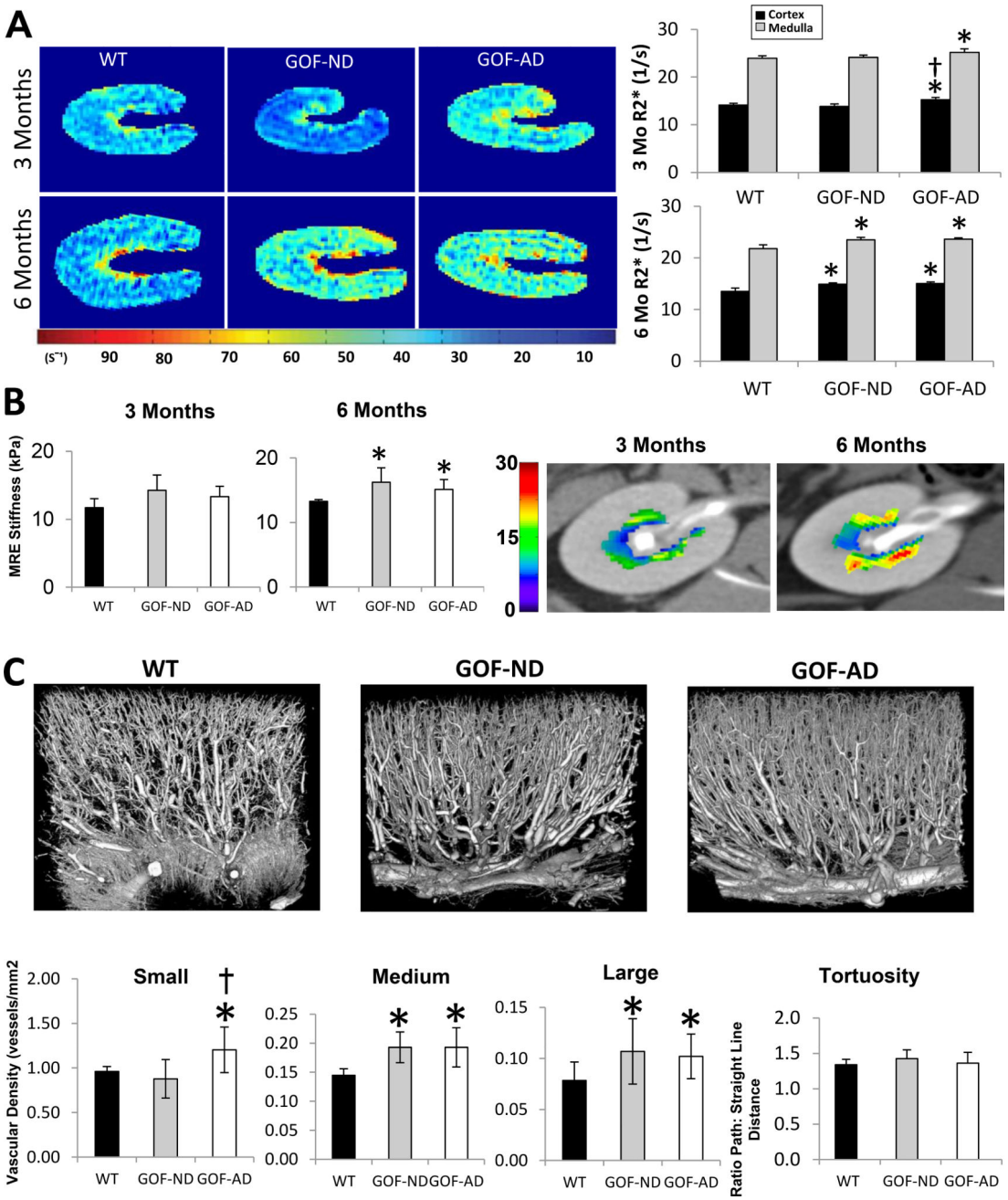

Figure 2.

(**A**) Single-kidney BOLD-MRI illustrating hypoxic regions (yellow-red). R_2* in the cortex and medulla increased in GOF-AD by 3-months on diet, and in GOF-ND by 6 months (n=7/group). (**B**) MRE showed in-vivo elevated renal medullary stiffness (yellow-red) at 6-month in both GOF groups (n=5/group). (**C**) Representative three-dimensional micro-CT images of kidney segments and quantification of renal microvascular spatial density and tortuosity, showing an increase in the microvascular density in GOF groups unchanged tortuosity. *p<0.05 vs. WT; †p<0.05 vs. GOF-ND.

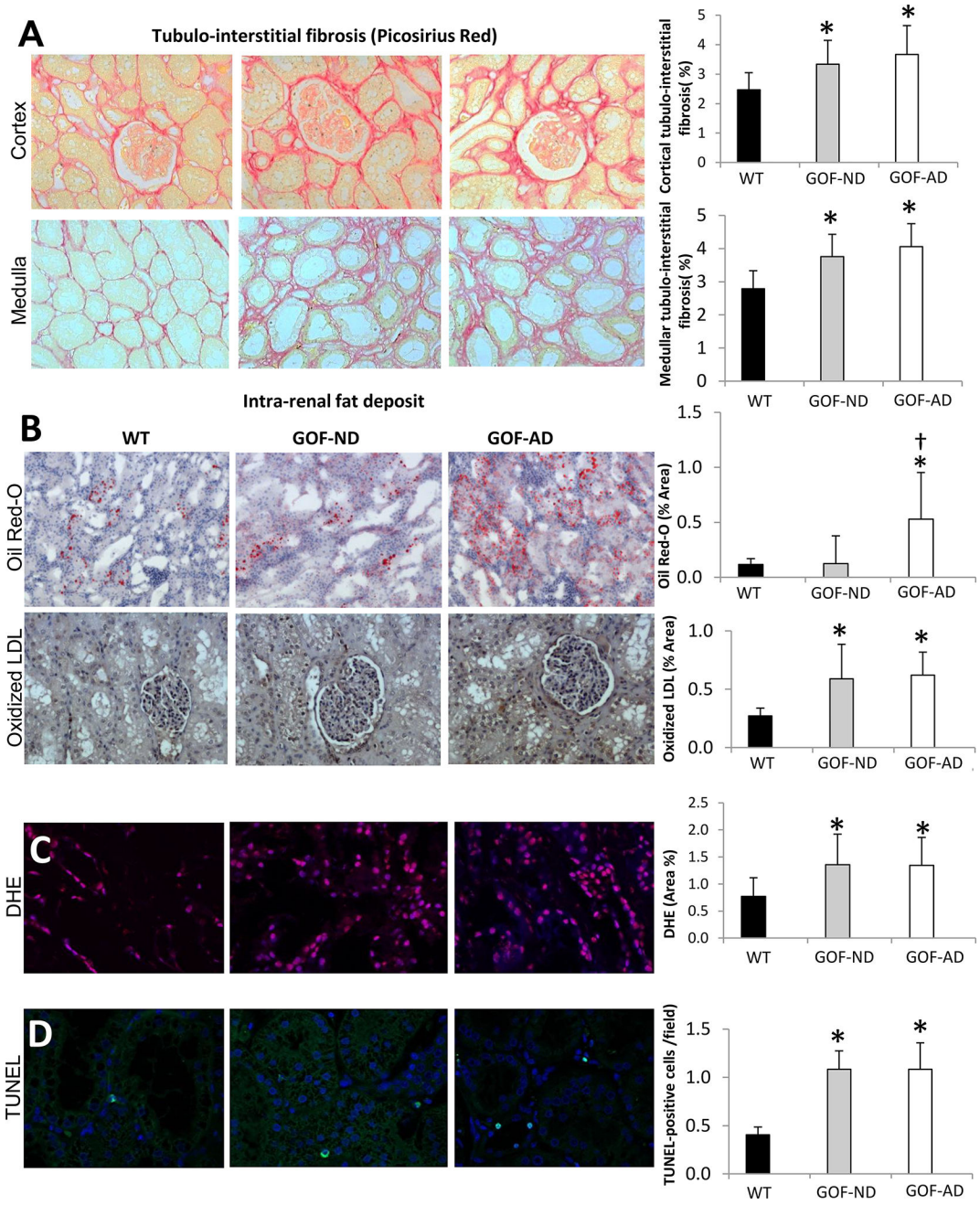

Figure 3.

(**A**) Cortical and medullary tubulointerstitial Picrosirius red staining showing increased fibrosis in GOF groups. (**B**) Intra-renal fat deposits (Oil-red-O) increased in GOF-AD, while tubulointerstitial Oxidized LDL (brown) accumulated in both GOF groups. (**C**) Renal production of superoxide anion (DHE, magenta) and (**D**) Apoptosis (TUNEL, cyan) increased in both GOF-ND and GOF-AD (n=7/group). *p<0.05 vs. WT; †p<0.05 vs. GOF-ND.

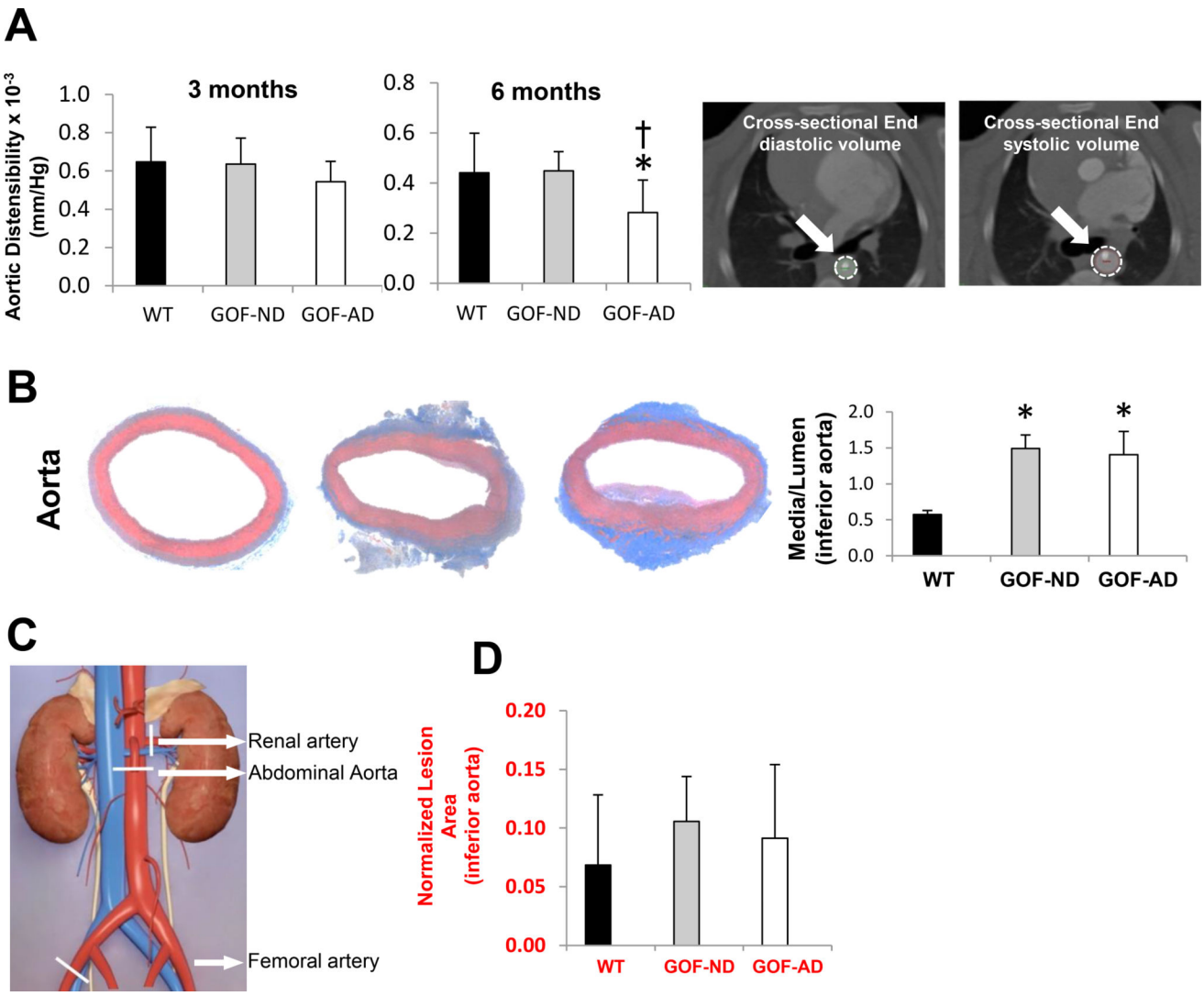

Figure 4.

(**A**) CT-determined distensibility showed a fall in aortic elasticity at 6 months. (**B**) Media-to-lumen ratio of the aorta increased in both GOF-ND and GOF-AD (n=7/group). (**C**) Diagram showing the harvested vessels location, marked with white line segments. (D) Histomorphometrical assessments of normalized lesion area in the inferior aorta were not significantly increased in the GOF groups. *p<0.05 vs. WT.

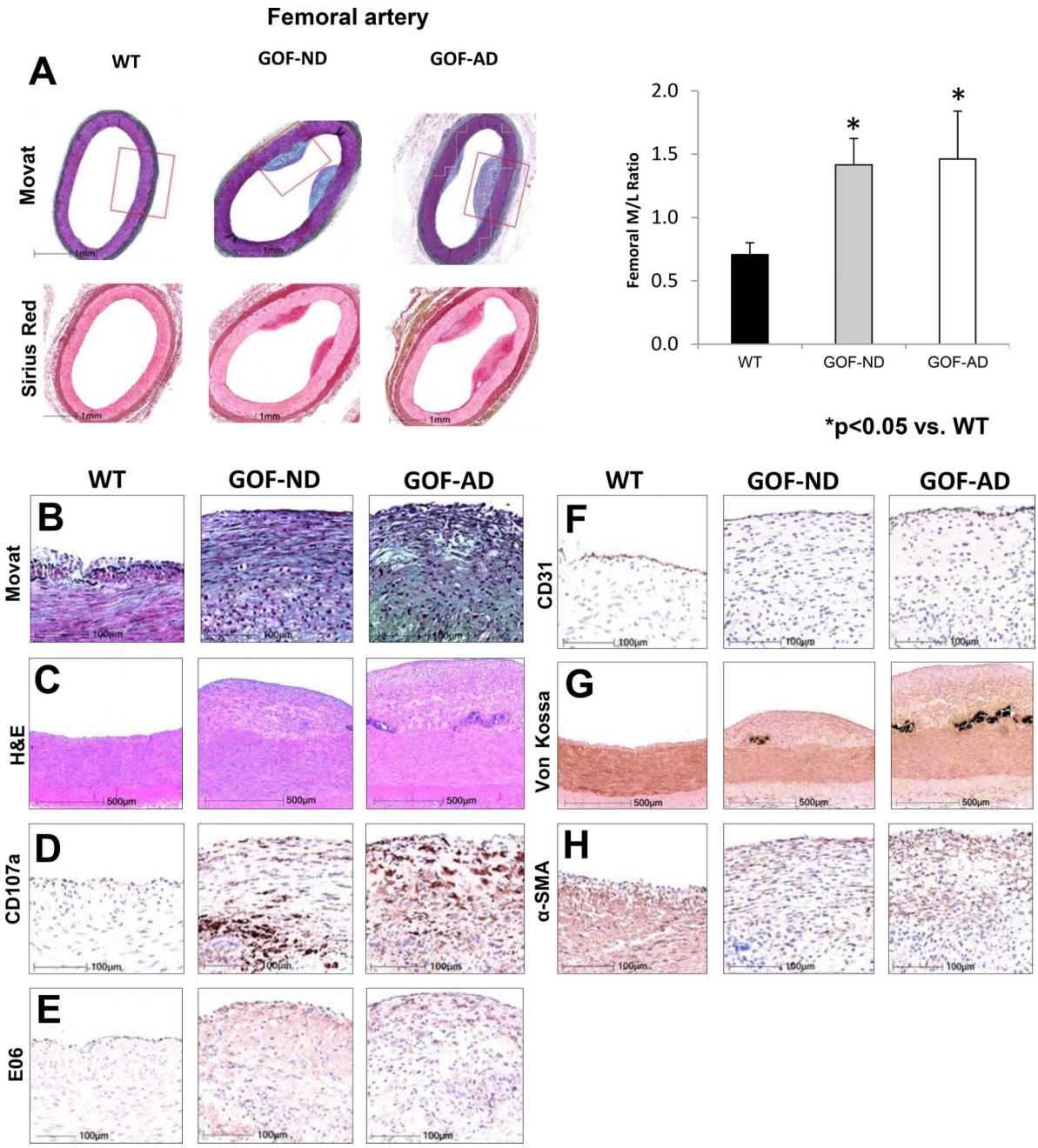

Figure 5.

Femoral arterial early lesions in GOF pigs. (**A**) Images and media-to-lumen ratio. (**B**) Movat, (**C**) H&E, (**D**) CD107a, (**E**) E06 (oxidized-LDL), (**F**) surface endothelium (CD31/PECAM-1), (**G**) Von Kossa (calcium), (**H**) and α-smooth muscle cell actin (a-SMA), showed increased staining in GOF-ND and GOF-AD (n=7/group). The higher power magnifications H&E and von Kossa represent regions corresponding to the red box in the low power Movat pentachrome stain. The minimal lesions in the WT mainly consisted of

smooth muscle cells and neointimal hyperplasia. Contrarily, fibroatheromatous plaques with oxidized LDL accumulation were noted in GOF-ND and GOF-AD. *p<0.05 vs. WT.

Table 1

Systemic and renal characteristics in wild type (WT) and GOF pigs fed a normal (ND) or atherogenic (AD) diet for 6-month.

Parameter	WT-ND		WT-AD	PCSK9 GOF-ND		PCSK9 GOF-AD	
	3-months	6-months	6-months	3-months	6-months	3-months	6-months
Body Weight (Kg)	50.7±3.1	65.6±4.6$^{\#}$	87.0±8.3	33.8±4.0	46.7±3.3$^{\#}$	40.9±1.3	58±2.4$^{\#}$
MAP (mmHg)	118.2±5.0	119.8±9.8	118.6±10.6	132.8±4.0*	137.3±8.0*	131.9±2.8*	133.8±4.4*
SVR (dynes·s/cm5)	2812±617	2900±514	2441±645	3794±433*	3592±520$^{*¥}$	3570±418*	3680±551$^{*¥}$
Lipid fractions (mg/dL)							
Total Cholesterol	76.7±24.5	83.71±20.9	312.3±13.0*	466.7±214.2*	434.4±47.2*	857.6±143.0*†	952.1±175.6*†
HDL-C	39.57±6.45	47.0±13.4	136.7±15.2*†	45.1±19.9	37.6±3.9	80.3±25.3*†	87.1±20.8*†
LDL-C	32.1±15.4	29.8±12.6	160.2±5.3*†	412.0±195.2*	388.8±45.6*	769.5±121.5*†	853.5±161.1*†
VLDL-C	2.9±1.3	3.92±2.0	15.5±4.4*†	7.1 ±1.9*	6.4±2.1	6.2 ±1.8*	9.21±1.6*†
Triglycerides	18.3±8.4	24.5±12.7	77.3±22.0*	44.2±11.6*	40.3±13.5	38.9±11.5*	57.6±10.1*†
Albumin/Creatinine Ratio	-	27.33±14	-	-	35.2±25	-	29.6±18
PCSK9 (ng/mL)	-	0.01±0.03	0.01±0.02	-	724±54$^{*¥}$	-	743±70$^{*¥}$
Perfusion (mL/min/cc)							
Cortex	4.2±0.3	3.7±0.2	5.8±0.9	4.2±0.3	4.4±0.2	4.2±0.4	4.1±0.6
Medulla	2.8±0.3	1.8±0.2	3.6±0.7	2.6±0.2	3.0±0.4	2.8±0.6	3.2±0.7
RBF (ml/min/cc)	4.1±0.23	4.2±0.4	5.6±0.5	4.0±0.2	4.1±0.1	4.1±0.3	4.0±0.4
GFR (ml/min/kg)	0.66±0.02	0.63±0.03	0.57±0.03	0.70±0.05	0.67±0.03	0.60±0.02	0.63±0.02
Tubular Injury Score	-	1.2±0.58	-	-	1.86±0.69*	-	1.57±0.53*

ANOVA yielded $p<0.05$ for all systemic measurements, but not for renal parameters.

$^{*}p<0.05$ vs. WT-ND,

$^{¥}p<0.05$ vs. WT-AD

$^{†}p<0.05$ vs. PCSK9 GOF-ND in the same time period,

$^{\#}p<0.05$ vs. Baseline (n=7 each group, except WT-ND with n=3).

GOF: Gain of function. MAP: Mean arterial pressure, RBF: Renal blood flow, GFR: glomerular filtration rate. SVR: Systemic vascular resistance, NS: Not significant. VLDL-C: Very low-density lipoprotein cholesterol; HDL-C: high-density lipoprotein cholesterol; LDL-C: low-density lipoprotein cholesterol.

Table 2

Summary of the parameters change with the duration of the diet.

	PCSK9 GOF-ND*		PCSK9 GOF-AD*	
	3-months	**6-months**	**3-months**	**6-months**
MAP (mmHg)	↑	↑	↑	↑
Total Cholesterol	↑	↑	↑	↑
HDL-C (mg/dL)	↔	↔	↑	↑
LDL-C (mg/dL)	↑	↑	↑	↑
Triglycerides (mg/dL)	↑	↔	↑	↑
Cardiac Output (L/min)	↔	↑	↔	↑
Perfusion (mL/min/cc)	↔	↔	↔	↔
RBF (ml/min/cc)	↔	↔	↔	↔
GFR (ml/min/kg)	↔	↔	↔	↔
Renal artery diameter (mm^3)	↓	↓	↓	↓
Plaque volume (mm^3)	↔	↔	↑	↑
MRE Stiffness (kPa)	↔	↔	↑	↑
Aortic Distensibility (mm/Hg)	↔	↔	↔	↓

* $p<0.05$ vs. WT;

MAP: Mean arterial pressure; RBF: Renal blood flow; GFR: glomerular filtration rate; MRE: Magnetic Resonance Elastography; HDL-C: high-density lipoprotein cholesterol; LDL-C: low-density lipoprotein cholesterol.